A holistic approach to Thermo-Mechanical Fatigue phase angle effects for an aerospace nickel superalloy

V. Gray[1,2], J. P. Jones[2], M. T. Whittaker[2], R.J. Lancaster[2], C. J. Pretty[2], and S. J. Williams[3]

1. School of Mechanical, Medical and Process Engineering, Science and Engineering Faculty, Queensland University of Technology, Brisbane, 4000, AUSTRALIA

2. Institute of Structural Materials, Swansea University, Crymlyn Burrows, Swansea, SA1 8EN, UK

3. Rolls-Royce plc, P.O. Box 31, Derby, DE24 8BJ, UK

Abstract

Thermo-Mechanical Fatigue (TMF) is one of the most complex mechanical phenomena that couples creep, fatigue and oxidation. So far, developing simple empirical relationships like those that exist in isothermal equivalents have proven elusive. This work presents a study on the TMF behaviour of the aerospace nickel based superalloy RR1000 using TMF fatigue crack growth rates, strain controlled TMF results, studies of the fracture morphologies and empirical lifing models. This paper takes a holistic approach to TMF lifing, specifically focusing on the impact of phase angle. As a result, this work develops an elastic modulus normalisation technique that when a Coffin-Manson type relationship is applied, predicts life of material under interim TMF phase angles.

1. Introduction

Components in aerospace engines experience complex stress-temperature conditions throughout their service life [1]. Therefore, designing components to withstand these conditions in ever higher performance engines, means going beyond characterising a material's isothermal properties [2]. As a life limiting factor in engine design, fatigue characterises a material's response to defined cyclical stress or strain under isothermal conditions. However, Thermo-Mechanical Fatigue (TMF) testing seeks to better characterise in-service behaviour of materials through applying both cyclic stress/strain and cyclic temperature conditions. The additional complexity of non-isothermal conditions is otherwise regarded as phasing or phase angle (ϕ) which quantifies the difference in cycles between the strain and temperature, focussing on strain controlled TMF (SC-TMF), as is most commonly utilised. The most common TMF cycles studied are In-Phase (IP, 0°) where strain (ε) and temperature *(T)* increase and decrease concurrently, and Out-of-Phase (OOP, 180°) where one increases as the other decreases.

Currently, there is limited understanding of the impact that cyclic temperature has on fatigue properties under TMF loading conditions. In the literature there are few investigations into TMF behaviour of superalloys, particularly polycrystalline

materials. Marchioni *et al.* examined Nimonic 90 where for higher ε, OOP tests produced longer lifetimes than IP tests [3]. When examined by Pahlavanyali *et al.* under an applied strain range ($\Delta\varepsilon$) of ±0.4%, the OOP life was almost 4 times longer than the IP, but at 0.3%, IP and OOP had similar lives [4]. In addition, work by Huang *et al.* [5] on M963 and Hyde *et al.* [6-7] on RR1000, suggest that T and ε influence IP and OOP lives to different degrees. Conceptually, comparing IP to OOP, the IP cycle should experience more damage as the highest strain coincides with peak temperature (T_{max}) and reduced modulus (E), yet that is not seen consistently in test data. Lancaster *et al.* proposed a model linking ε and ϕ although this was limited to the variation of ϕ at a single $\Delta\varepsilon$ [8].

Based on the previous work on RR1000 specifically, it can be seen that TMF life is dependent on a currently undefined relationship between phase angle and strain range. For IP and OOP tests of $\Delta\varepsilon$=0.8-1.4% and T= 300-700°C, the OOP cycle showed a longer life than IP for $\Delta\varepsilon$>1%, but was reversed at lower $\Delta\varepsilon$ [9]. SC-TMF tests performed at phase angles between IP and OOP showed a consistent increase in TMF life for $\Delta\varepsilon$=1% when phase angle progresses from IP to OOP [10]. Examining the mean stress of these tests under stabilised conditions ($\sigma_{1/2\ life\ mean}$), for CW and IP angles it became more compressive, and, for ACW and OOP angles more tensile, suggesting a potential correlation between $\sigma_{1/2\ life\ mean}$ and TMF life [10]. For shorter TMF tests, TMF life is no longer dominated by crack initiation and therefore these authors examined TMF crack propagation. Having built new TMF crack propagation facilities, load control TMF (LC-TMF) crack growth tests were conducted [11, 12]. Microstructural observations showed that the LC-TMF IP test exhibited intergranular cracking similar to the 700°C isothermal test. For OOP tests, transgranular cracking was primarily observed, similar to that seen in the 300°C isothermal fatigue test [11]. The 90CW specimen showed mixed mode failure [13]. Jones et al. examined IP and OP TMFCG behaviour and identified that peak stress-temperature combinations defined by the TMF phase angle are highly influential on the material behaviour i.e. plasticity, and therefore material life [13].

Currently, the impact of TMF phase angle on failure mechanisms is somewhat understood, but a mathematical relationship linking TMF phase angle, strain and life remains elusive. For Nimonic 90, OOP tests were conducted with relative phase angle variations of -20°, -10°, +10° and +20° [14]. A small phase angle variation of +/-10° did not produce any measurable difference in life, but at +/-20° there was a small effect linked to a change in plasticity resulting from stress-temperature timing [14]. For Mar-M247, a range of phase angles were examined over different strain ranges. For $\Delta\varepsilon$=0.3-0.6% IP, 90CW, 90ACW and OOP phase angles were explored [15]. Although, understanding of the mechanisms was achieved, a relationship between the phase angle was not determined. This was similar to the investigation of IN617 where IP, 90CW, 90ACW and OOP phase angles were explored for $\Delta\varepsilon$=0.3-0.5%, and damage mechanisms were identified but a relationship was not established [16]. Despite the numerous investigations by these authors on RR1000, a holistic view of

TMF phase angle life using a Basquin approach to derive a S-N curve for SC-TMF that used some preliminary TMFCG results for insight into the impact of oxidation, also could not characterise the relationship between TMF phase angle, strain and life [8].

As an experimentally challenging testing technique, TMF introduces a complexity through thermal cycling that is not well understood. From previous works there is some limited understanding of the microstructural impact thermal cycling has on a material's fatigue response. Due to this limited knowledge, these investigations have yet to produce a relationship to predict TMF life, either from equivalent isothermal tests, or a subset of TMF phase angles. This paper focuses on developing a more holistic approach to understanding TMF phasing from expanded test data, and, developing a relationship that relates the life seen at one phase angle to life seen at another.

2. Experimental methods:

RR1000 is a γ' strengthened polycrystalline Ni-based superalloy with composition shown in Table 1. It is produced via powder metallurgy and strengthened through secondary γ' phase precipitation of $Ni_3(Al, Ti, Ta)$ within an FCC γ matrix. The γ grain size in this study was 4-8μm, resulting from a sub-solvus solution heat treatment that left irregular shaped 1-5μm primary γ' particles on grain boundaries. The microstructure is presented in Figure 1.

Table 1: RR1000 Composition (%wt)

Ni	Cr	Co	Mo	Ta	Al	Ti	Hf	C	B	Zr
Bal.	15	18.5	5.0	2.0	3.0	3.6	0.5	0.03	0.02	0.06

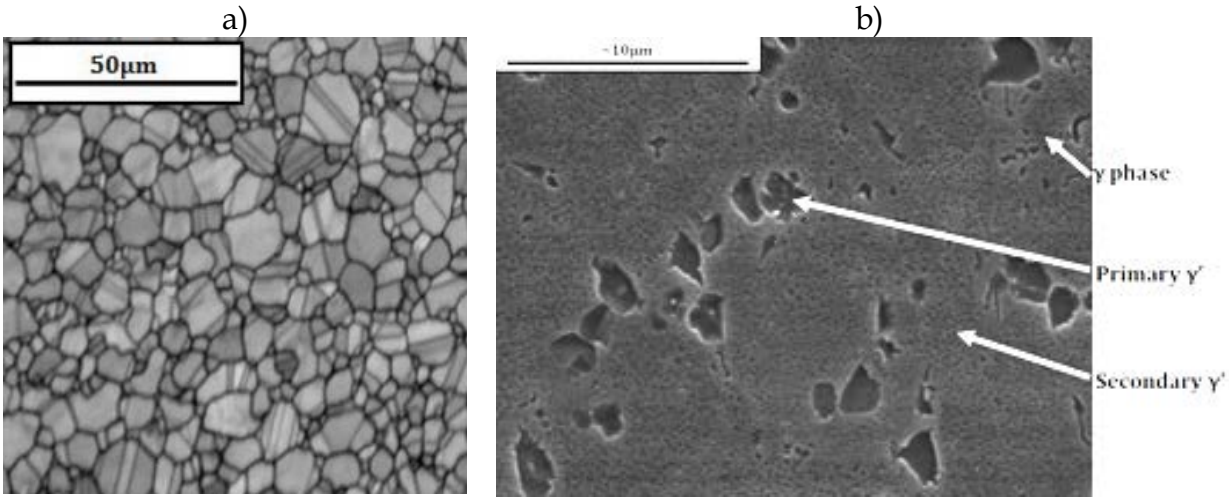

Figure 1: RR1000 Microstructure a) Electron Backscatter Diffraction (EBSD) of grain structure, and b) Scanning Electron Microscopy (SEM) of precipitates

Although IP and OOP cycles are the most well studied TMF cases, they represent the most extreme cases of TMF loading and other phase angles, ϕ, need to be considered as they are more representative of in-service conditions [8]. Figure 2 illustrates the additional TMF ϕ considered in this and previous work; ϕ=45CW (+45°), 90CW (+90°), 90ACW (-90°), and 45ACW (-45°). Clockwise cycles denoted by CW, experience peak strain (ε_{max}) as T is increasing, whereas anticlockwise (ACW) cycles experience ε_{max} when T is decreasing.

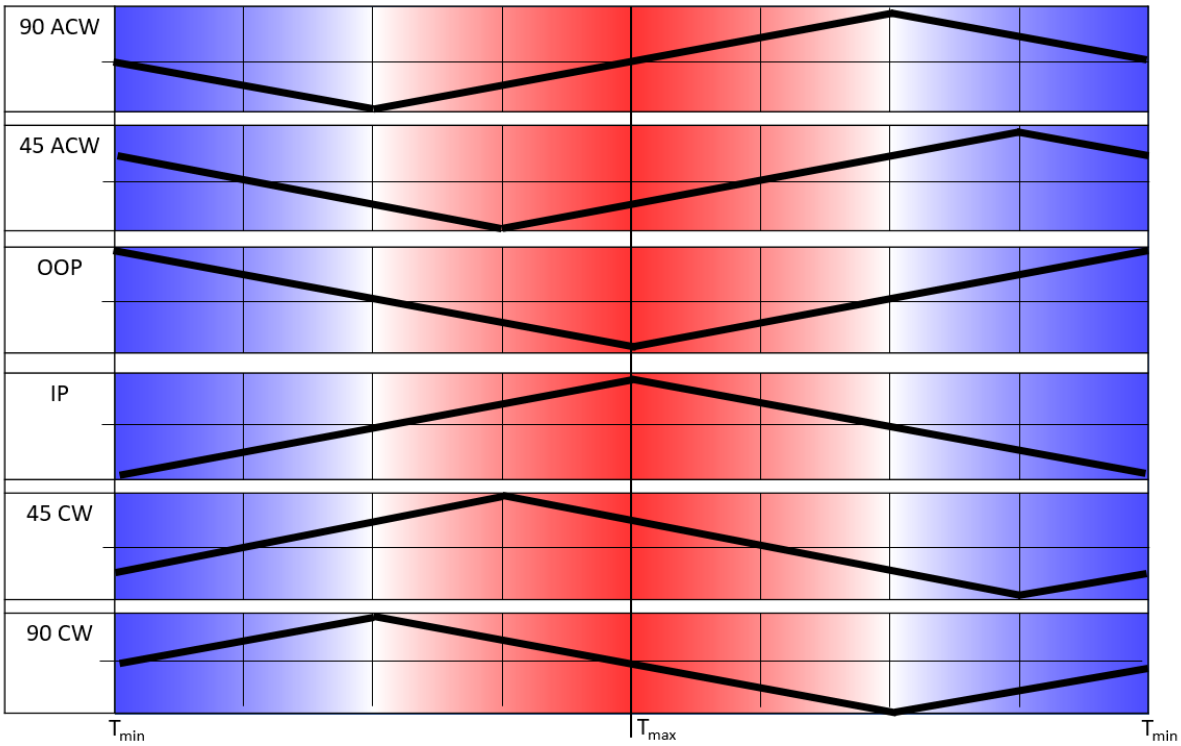

Figure 2: TMF Phase Angle Strain Profiles (Black = Strain, Red/Blue = Temperature)

SC-TMF tests were conducted using a tubular hollow test specimen described in [17] where the machined surface was finished with a longitudinal polish to avoid premature crack initiation from surface features. Testing was conducted according to the guidelines in the strain controlled TMF Code of Practice [18], although the specimen geometry is non-standard. The tests were designed to follow an initial constant path through strain-temperature space as shown previously [17]. This results in varying R ratio across phase angles, from R=0 for IP tests, R=-1 for CW90 and ACW90 tests, and R=-∞ for OOP tests. Pre-test modulus checks, thermal compensation definitions and zero stress trials were also performed to ensure test viability. Tests were performed on an ESH 100kN tension-torsion capable servo-hydraulic test machine using radio-frequency (RF) induction heating through a water cooled copper coil. Specimens were air-cooled by passing air through the hollow specimen and by directed air onto the outer surface. An IMPAC IP10 optical pyrometer and 12mm gauge MTS high temperature extensometer was used with the

strain and thermal cycles synchronised by a closed loop computer. Failure was defined to have occurred when a 10% drop from ½ life peak stress was recorded. A summary of the strain control tests conducted is provided in Table 2.

Table 2: Test conditions for strain control fatigue tests.

Applied Phase Angle	Strain Range	Temperature Range		Applied Phase Angle	Strain Range	Temperature Range
(°)	(%)	(°C)		(°)	(%)	(°C)
0 (IP)	1.40	300-700		90 (CW)	1.40	300-700
0 (IP)	1.20	300-700		90 (CW)	1.20	300-700
0 (IP)	1.00	300-700		90 (CW)	1.00	300-700
0 (IP)	0.90	300-700		90 (CW)	0.80	300-700
0 (IP)	0.85	300-700				
0 (IP)	0.80	300-700				
0 (IP)	0.80	300-700				
180 (OOP)	1.40	300-700		90 (ACW)	1.40	300-700
180 (OOP)	1.20	300-700		90 (ACW)	1.20	300-700
180 (OOP)	1.00	300-700		90 (ACW)	1.00	300-700
180 (OOP)	0.90	300-700		90 (ACW)	0.80	300-700
180 (OOP)	0.80	300-700				
45 (CW)	1.40	300-700		135 (ACW)	1.40	300-700
45 (CW)	1.20	300-700		135 (ACW)	1.20	300-700
45 (CW)	1.00	300-700		135 (ACW)	1.00	300-700
45 (CW)	0.80	300-700		135 (ACW)	0.80	300-700

LC-TMF crack propagation tests were conducted on an Instron 1362 electric screw testing system with σ_{max}=450MPa under R=0.1. A solid specimen was used with a 20mm gauge length and 5x5mm square cross section (see [10] for specimen geometry). The as machined surface had a 0.22mm starting notch introduced, manufactured using a mechanical cutting technique with a diamond edged saw. Specimens were pre-cracked first at room temperature and then at the temperature at which maximum stress occurred in the TMF cycle, to reduce any notch effects. Induction heating coupled with fan cooling was used to achieve the 300-700°C 80 second thermal cycle with a heating/cooling rate of 10°C/s [12]. The Direct Current Potential Drop (DCPD) method was used to measure the crack growth with an applied current of 15 Amps.

Isothermal fatigue tests were conducted at T=300, 500 and 700°C for R=0.1 with σ_{max}=450MPa and compared to IP, 90CW, 90ACW and OOP LC-TMF with the same stress range ($\Delta\sigma$) and T=300-700°C [11]. A summary of the crack propagation tests conducted is provided in Table 3.

Table 3: Test conditions for load control fatigue crack propagation tests.

Applied Phase Angle	Applied stress	Temperature Range
(°)	(MPa)	(°C)
0 (IP)	450	300-700
90 (CW)	450	300-700
90 (ACW)	450	300-700
180 (OOP)	450	300-700
Isothermal	450	300
Isothermal	450	500
Isothermal	450	700

3. Results

Figure 3a shows the SC-TMF results for six phase angles with $\Delta\varepsilon$ ranging from 0.8-1.4%. Some results were from previous experiments [19]. New results in Figure 3a include $\Delta\varepsilon$=0.75, 0.85 and 0.9% for IP and $\Delta\varepsilon$=0.9% for OOP. Figure 3b shows the LC-TMF crack growth rates of four phase angles again normalised by the IP results. For each condition three TMF tests were completed to establish consistency. The data provided in Figure 3b was deemed to be representative of that condition. It should be noted that the shallower gradient exhibited by the 90CW test is a clear example of the dominance of a single damage mechanism (in this case oxidation ahead of the crack tip driving crack growth) and has been detailed further in previous work [11].

The combination of the total life results from the strain control data, and a propagation life from the crack propagation data can then be used to derive a holistic approach to TMF life prediction.

a)

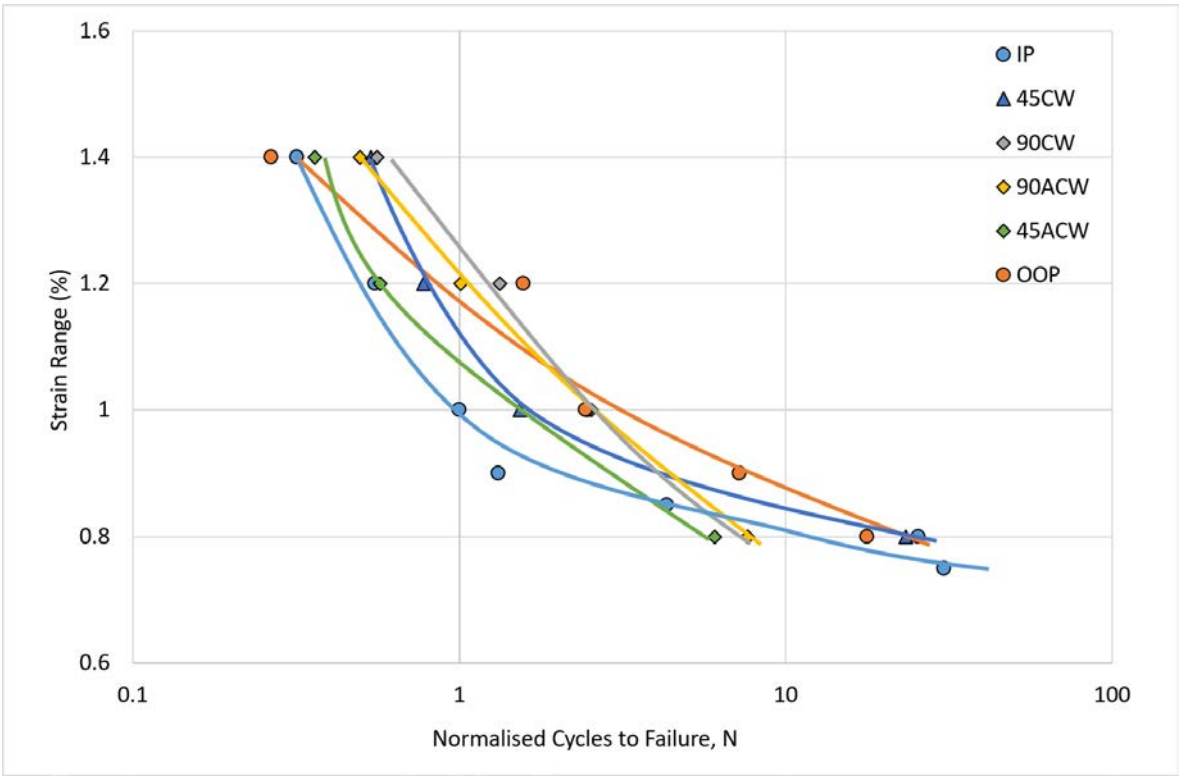

b)

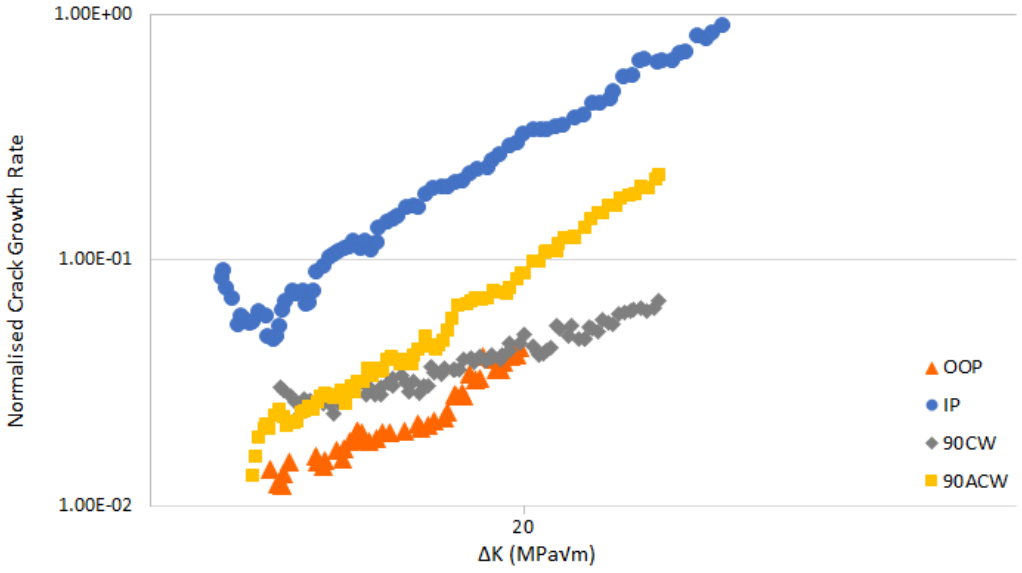

Figure 3: Phased Thermomechanical Fatigue Results, a) Strain Controlled TMF, and b) Load Controlled TMF crack growth

3.1. Crack Initiation and Propagation Analysis

For TMF, the crack initiation or crack propagation rate depends upon the specific ε-T conditions that are defined by the phase angle. The complexity of the ε and thermal cycles means that phased TMF is a combination of fatigue, creep and environmental damage that ultimately defines the fatigue life, N. In simple terms, the total fatigue life is the summation of life cycles spent in crack initiation and propagation such that:

$$N = N_i + N_p \tag{1}$$

From the LC-TMF tests, Paris constants (C and m) were obtained for each phase angle which can be used to predict the fatigue life spent in propagation by integration of the Paris Law.

$$\frac{da}{dN} = C\,\Delta K^m \tag{2}$$

$$N_p = \int_{a_0}^{a_f} \frac{da}{C\,\Delta K^m} = \frac{1}{C\left(Y\,\sigma\sqrt{\pi}\right)^m}\left[\frac{a_f^{m'} - a_0^{m'}}{m'}\right] \tag{3}$$

where a_0 and a_f are the initial and final crack lengths, Y is the geometry factor, and $m' = \left(1 - {}^{m}/_{2}\right)$. To apply Eq. 3, the initial crack size a_0 was taken to be equal to the Equivalent Initial Flaw Size (EIFS). For RR1000 it was found using a Weibull distribution that 98% of EIFS will be <65μm [20]. Using Eq. 3, SC-TMF failure was defined as when a drop in ½ life peak stress ($\sigma_{1/2\ life\ max}$) of 10% was observed, which corresponds with $a_f \approx 1$mm. Therefore, estimations of the crack propagation phase have been made assuming this initial EIFS.

Clearly, under strain control conditions however, it is recognised that the stress will evolve throughout the test. As a first order assumption for these calculations, the applied stress has been assumed to be the stabilised tensile stress at the half-life condition ($\sigma_{1/2\ life\ max}$). The compressive part of the cycle has not been considered since previous work has indicated that it has little influence on the crack growth rate under these conditions [21].

The predicted time spent in propagation for the SC-TMF tests based on Eq. 3 and the LC-TMF Paris constants are compared to the striations seen on the fracture surfaces of the SC-TMF samples. Using a Philips XL30 SEM, striations were counted and their distances measured using a REICHERT JUNG MeF3 optical microscope. The fracture surface and striations of SC-TMF 1% 90CW are shown in Figure 4 and all values listed in Table 2. Previous work provides greater detail of the methodology for these striation counts, including [22] continuous counts linearly outwards from the primary initiation site to ensure the striations relate to the dominant crack.

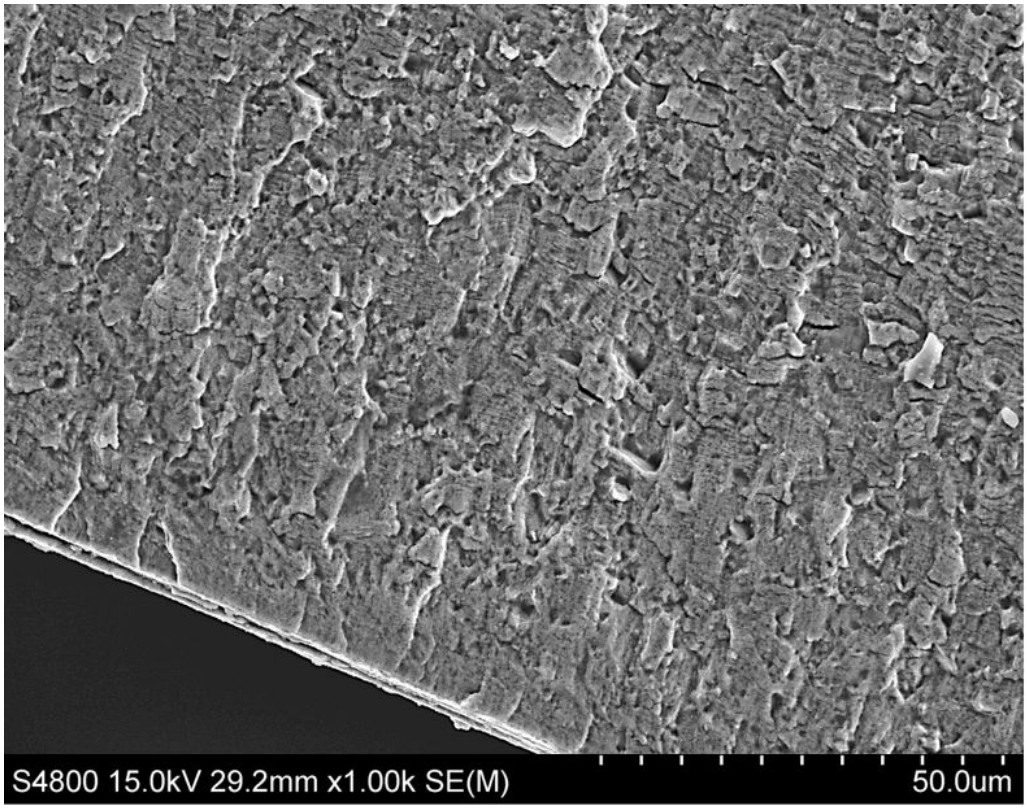

Figure 4: Fracture surface and striations of SC-TMF 1% 90CW

Table 2: Crack Propagation Life for SC-TMF: Normalised Striation Counts ($N_{striations}/N_{total}$)

	Strain Range			
	1%		1.40%	
Phase	*Striations*	*Paris Law*	*Striations*	*Paris Law*
90CW	0.27	0.27	0.99	1.00
90ACW	0.47	0.36	0.99	1.00
OOP	0.81	0.63		

Looking at Table 2 it can be seen that as $\Delta\varepsilon$ increases the amount of life spent undergoing crack propagation increases, as shown by $\Delta\varepsilon$=1.4% with TMF life being dominated by crack propagation. Comparing the calculated and measured growth rates for $\Delta\varepsilon$=1% it can be seen that the crack propagation life based on striation counts exceeds that based on Eq.3. However, typically the first 5% of the cycles in strain control tests are spent transitioning from the initial stress to the ½ life stress condition. Having used the ½ life stress values for the integrated Paris Law, this can account for the difference between the predicted and observed N_p at 1%. In a more detailed calculation the use of the evolving stress to characterise the stabilisation of the stress would effectively reduce the Paris Law prediction of N_p for 90CW and increases it for

90ACW and OOP, leaving these calculated lives more in line with the results found from the striations.

Considering this, the fatigue data seen here can be rationalised in the following way. As shown in Table 2 and from Eq. 3 for tests with $\Delta\varepsilon$>1%, the TMF life begins to become dominated by crack propagation with initiation occurring at ever earlier fractions of the total life. It can be seen that the TMF lives of the 90CW, 90ACW and OOP cycles are directly related to the crack growth rates for these phase angles. Specifically, from Figure 3b, the fastest crack growth rates tend to show the shortest lives at $\Delta\varepsilon$=1.4 and 1.2%, which is expected from the crack growth rates if the TMF life is dominated by propagation. The 45CW phase angle tests also fit well with this approach, however, the 45ACW tests tend to show shorter fatigue lives than would be expected. Arguably, this may simply be due to the premature failure of a single test at $\Delta\varepsilon$=1.2% and unfortunately no crack propagation data is currently available for this phase angle to further investigate the cause of these reduced TMF lives.

As $\Delta\varepsilon$ decreases to 1% and lower, a more significant portion of TMF life is spent in crack initiation. In previous work [10], this has been linked to mean stress influences on TMF lives. Figure 5 highlights that at $\Delta\varepsilon$=1%, there is a greater spread in the mean stress values of differing phase angles than at higher strain ranges ($\Delta\varepsilon$=1.4%). At $\Delta\varepsilon$=1.4% there is a lower spread in mean stresses since the shorter lives allow less time for mean stress evolution away from zero, where it typically begins in an R=-1 test. This therefore means that, combined with the early crack initiation, calculating TMF life based only on R=0 crack propagation data in these high strain tests is a reasonable assumption. However, at $\Delta\varepsilon$=1% and below, the picture is different. Crack initiation now dominates over propagation and it is necessary to alter the approach. At this lower strain range, stress evolution is reduced, meaning that the mean stress now contributes more strongly to the overall life, and a relationship between mean stress and TMF life exists.

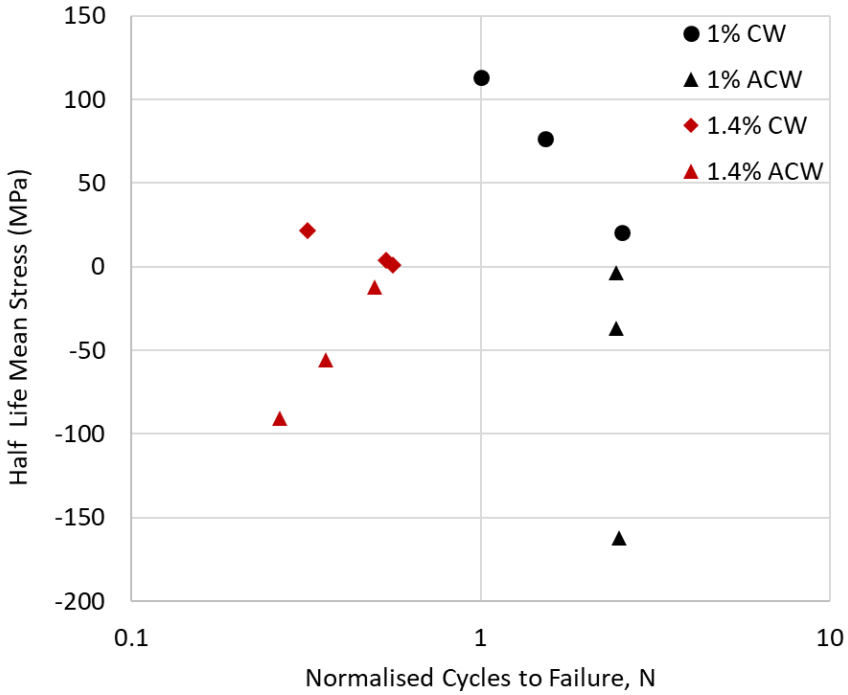

Figure 5: Normalised Mean Stress of Δε=1 and 1.4% for CW and ACW

Although mean stress has some correlation with life spent in crack propagation and overall life, it does not provide a simple empirical relationship. In previous work [19], the authors observed that the smaller the applied strain range, the greater and longer the stress evolution was during the test. The most extreme case was observed for the $\Delta\varepsilon$=0.8% where there was no stabilised mean stress for either the IP or OOP phases. The mean stress continued to evolve each cycle to reach +/-350MPa and did not stabilise. Some evidence of this lack of stabilisation was also seen in the $\Delta\varepsilon$=1% IP and OOP phases too. Interestingly, the 45CW, 90CW, 45ACW and 90ACW were more likely than the IP and OOP phases to develop a stabilised mean stress. In all cases higher strains also encouraged stabilisation of the mean stress.

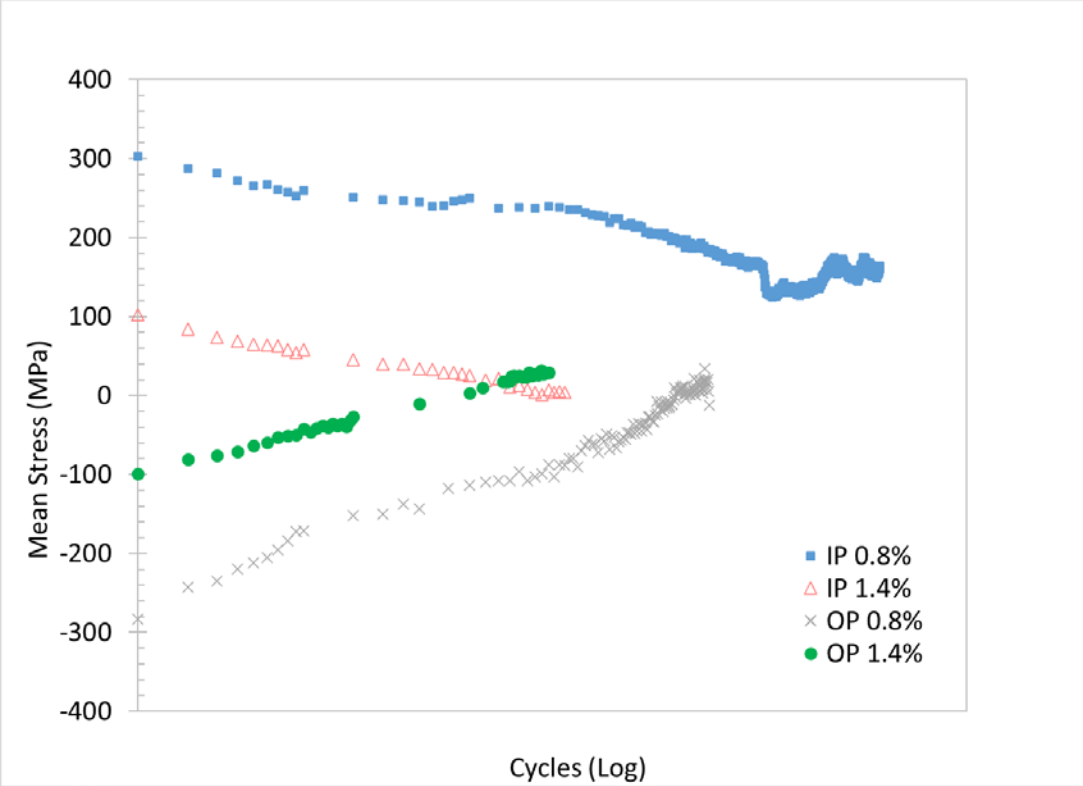

Figure 6: Mean stress evolution of IP and OOP tests at 0.8% and 1.4%

3.2. *Intergranular and Transgranular Failure*

As discussed, the phenomena of TMF cannot be understood from crack initiation and propagation behaviour alone. One of the consistent observations made for both SC-TMF and LC-TMF is that phase angle and failure mechanisms are strongly related. With an increasing phase angle there is a progression from intergranular to transgranular failure such as that seen in Figure 6. This is because the temperature at which the crack is fully open under tensile loading begins to fall, and time dependent mechanisms such as creep and oxidation exert less influence on weakening grain boundaries. Evidence of this has previously been shown [11]. For RR1000, isothermal fatigue at 650°C shows evidence of slip bands and dislocation climb [25] resulting in transgranular cracking along the {111} plane arising from localised planar deformation.

a) b)

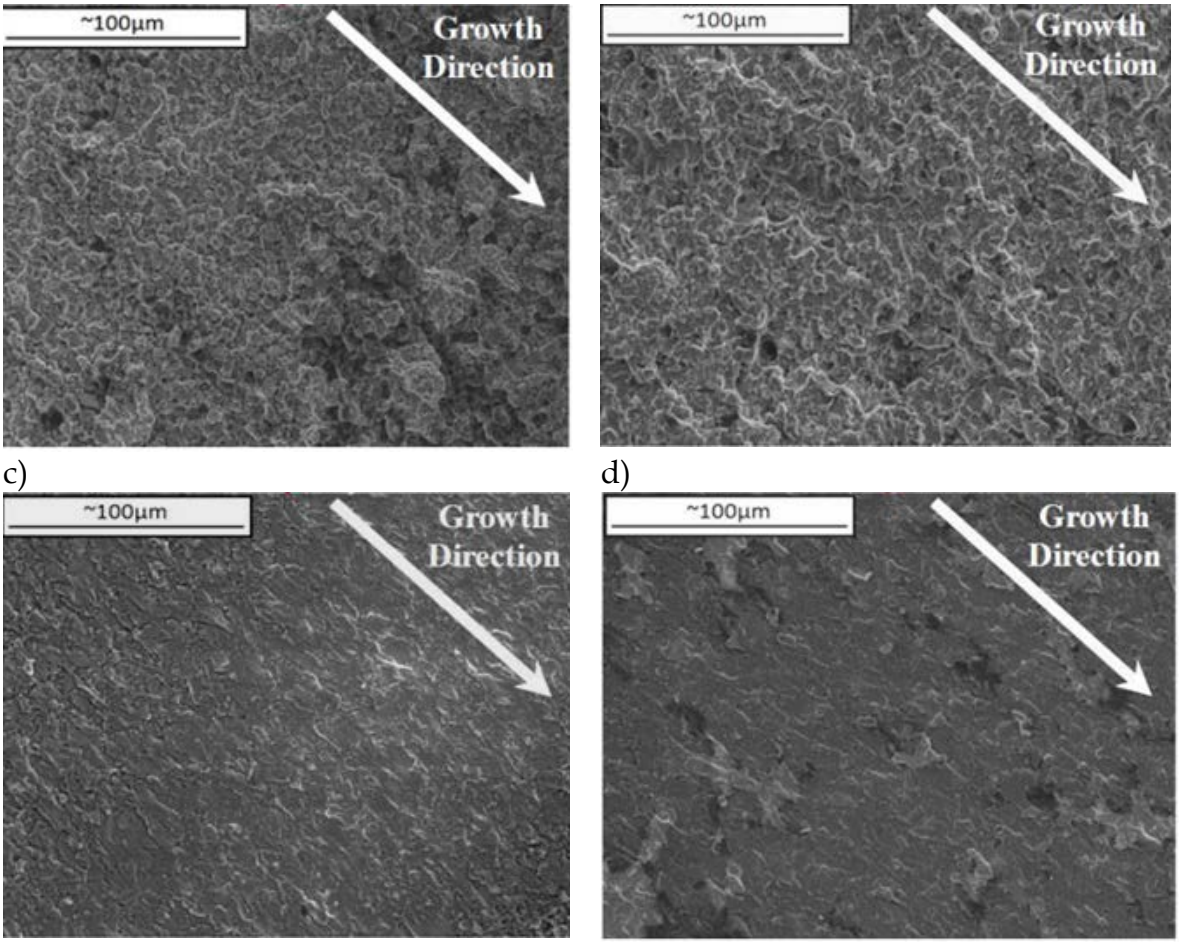

Figure 6: LC-TMF fracture surfaces; a) IP: intergranular, b) 90CW: mixed mode, c) 90ACW: transgranular, and d) OOP: transgranular

Considering the crack paths shown for each phase angle, as presented in Figure 6, it becomes possible to describe the effect of phase angle and oxidation. Although very little oxidation was observed on these test specimens, the dynamics of stress and temperature driven oxidation behaviour can be seen. Under IP conditions, σ_{max} and T_{max} occur simultaneously allowing for increased grain boundary diffusion of oxygen, weakening those grain boundaries and encouraging intergranular cracking. For OOP, although accelerated oxidation is expected under compression for nickel alloys as well [23], oxidation shows little effect on crack growth with a transgranular crack path observed, presumably due to the fact that oxidation penetration is restricted when the crack is closed at high temperature.

The impact of phase angle on oxidation and TMF life is most interesting in the comparison of 90CW and 90ACW. Both these phases show mixed mode failure but the 90CW appears more intergranular whereas the 90ACW is more transgranular (Figure 6). However, these effects have been rationalised by Pretty *et al.* [11]. Looking at Figure 7 it shows that for CW tests, the specimen unloads at high T allowing for oxidation at the crack tip, and hence promoting intergranular fracture when the specimen is reloaded at intermediate temperatures in the next cycle. Conversely in the ACW test, the specimen unloads at low temperatures, and so this oxidation does not

occur. Instead, dynamic transgranular cracking occurs more quickly than oxidation as the crack opens at higher T, and the failure mode remains transgranular.

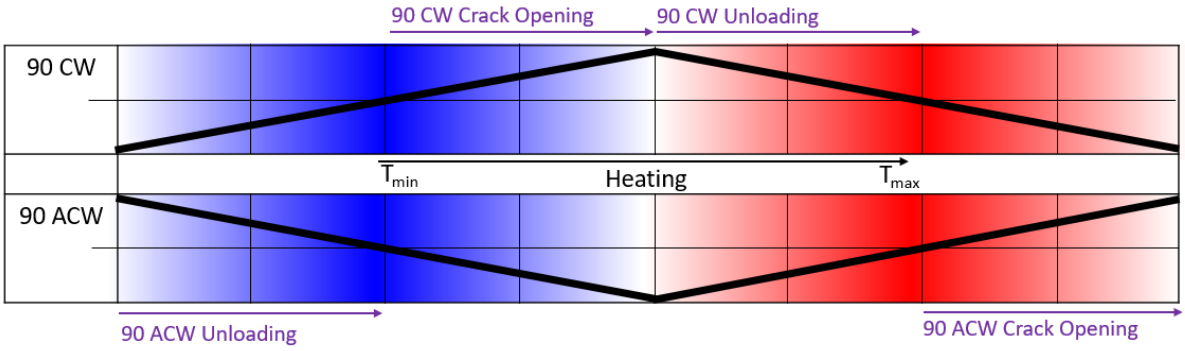

Figure 7: TMF Loading and Crack opening for 90CW and 90ACW.

4. Modelling

The role of crack initiation and propagation, as well as intergranular and transgranular failure in TMF is largely dependent on the behaviour of oxidation under the cyclic stress and temperature conditions imposed. This complicated relationship has meant that it is very difficult to link TMF results to isothermal data. For isothermal fatigue, lifing approaches fall into either stress-based or strain-based methods. Having observed there is a clear relationship between ½ life stress range ($\Delta\sigma_{1/2\ life}$) and ϕ, a Basquin model was proposed and applied to a limited dataset. The initial fitted constants were σ'_f=989.5 and b=-0.0818 found for $\Delta\varepsilon$=1% IP and OOP data [11].

In order to use a Basquin relationship to life TMF behaviour, ($\Delta\sigma_{1/2\ life}$) needs to be known. The proposed method of determining ($\Delta\sigma_{1/2\ life}$ would use the Mroz cyclic work hardening model [23] to predict the hysteresis loop for a user defined $\Delta\varepsilon$ and TMF phase angle. This approach has been shown to produce accurate ½ life stress-strain loops for defined TMF phases where the Basquin model no longer produces a sufficiently accurate fit to predict TMF life especially for the case of IP [10].

In Figure 8, this same analysis is expanded to include the results for all strains $\Delta\varepsilon$=0.8-1.4%. The Basquin model is applied to all SC-TMF data listed in this work and provides a fit where σ'_f=2084.9 and b=-0.1006.

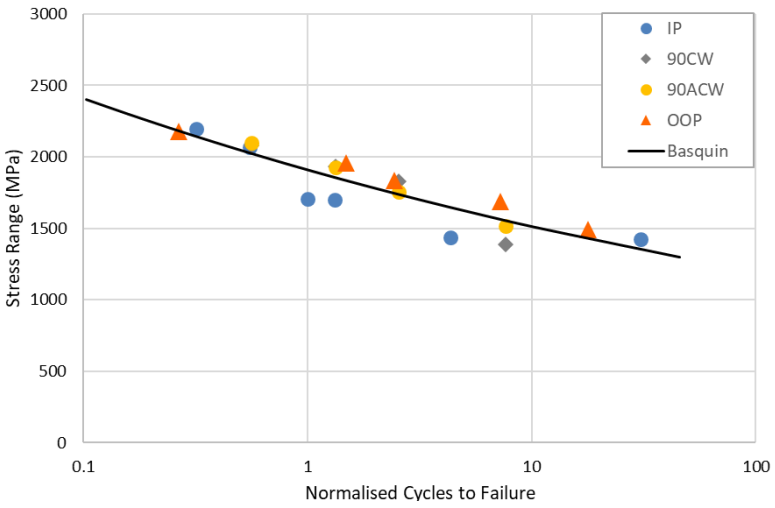

Figure 8: Basquin Model applied to SC-TMF data

From Figure 8, when more TMF data from greater strain ranges and more phase angles is considered, the Basquin model no longer performs as well as reported by Whittaker *et al*. [10]. Of concern is the poor fit for IP TMF and the general lack of convergence onto a single line for the range of phase angles investigated. This shows that a different approach needs to be taken, in order to relate one phase angle to another.

Considering the data shown in Figure 3, it spans a significant $\Delta\varepsilon$ from 0.7-1.4%. In order to develop a method of modelling TMF phasing, the relationship of stress and temperature needs to be characterised. As such, the phase temperature or the temperature at σ_{max} can be defined as:

$$T_{\varphi} = T(\sigma_{max}) = f(\varphi) \tag{5}$$

From analysis of the hysteresis loops for the testing conditions described, it is found that most of the deformation experienced is elastic. This is seen in Figure 9.

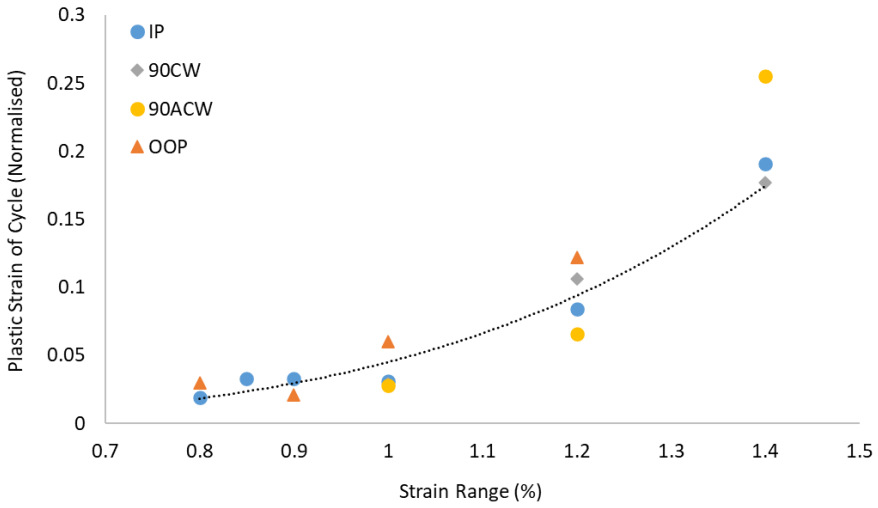

Figure 9: TMF plastic strain from ½ life hysteresis loops

As the majority of deformation is elastic, the analysis initially focuses on the elastic response of the material under different TMF phase angles. Under each phase angle, σ_{max} occurs at a different T and therefore different E. The T dependant E at σ_{max} is therefore phase angle dependant such that:

$$\Delta\varepsilon \approx \frac{\Delta\sigma}{E} \rightarrow \Delta\varepsilon_{\varphi} = \frac{\Delta\sigma\left(T_{\varphi}\right)}{E\left(T_{\varphi}\right)} \tag{6}$$

Considering this relationship, the phase angle dependency of the data in Figure 3 can be removed by accounting for σ_{max} and E at T. Therefore, ε can be modified to incorporate the difference in T at σ_{max} /ε_{max}:

$$\Delta\varepsilon\left(T_{\varphi}\right) = \frac{\Delta\sigma}{E\left(T_{\varphi}\right)} = \Delta\varepsilon\frac{E}{E\left(T_{\varphi}\right)} \tag{7}$$

where $\Delta\varepsilon(T_{\varphi})$ is the modified strain which is equal to $\Delta\varepsilon$ (the original test strain range) multiplied by the ratio of the chosen reference modulus (E at 500°C) divided by $E(T_{\varphi})$ (E at the T_{max}). By conducting this transform, the strain range is now comparable via the phase temperature modified strain term, $\Delta\varepsilon\left(T_{\varphi}\right)$.

In Figure 10 the data from Figure 3 is replotted using the phase temperature modified strain. Although no obvious relationship is apparent this transformation has a significant impact.

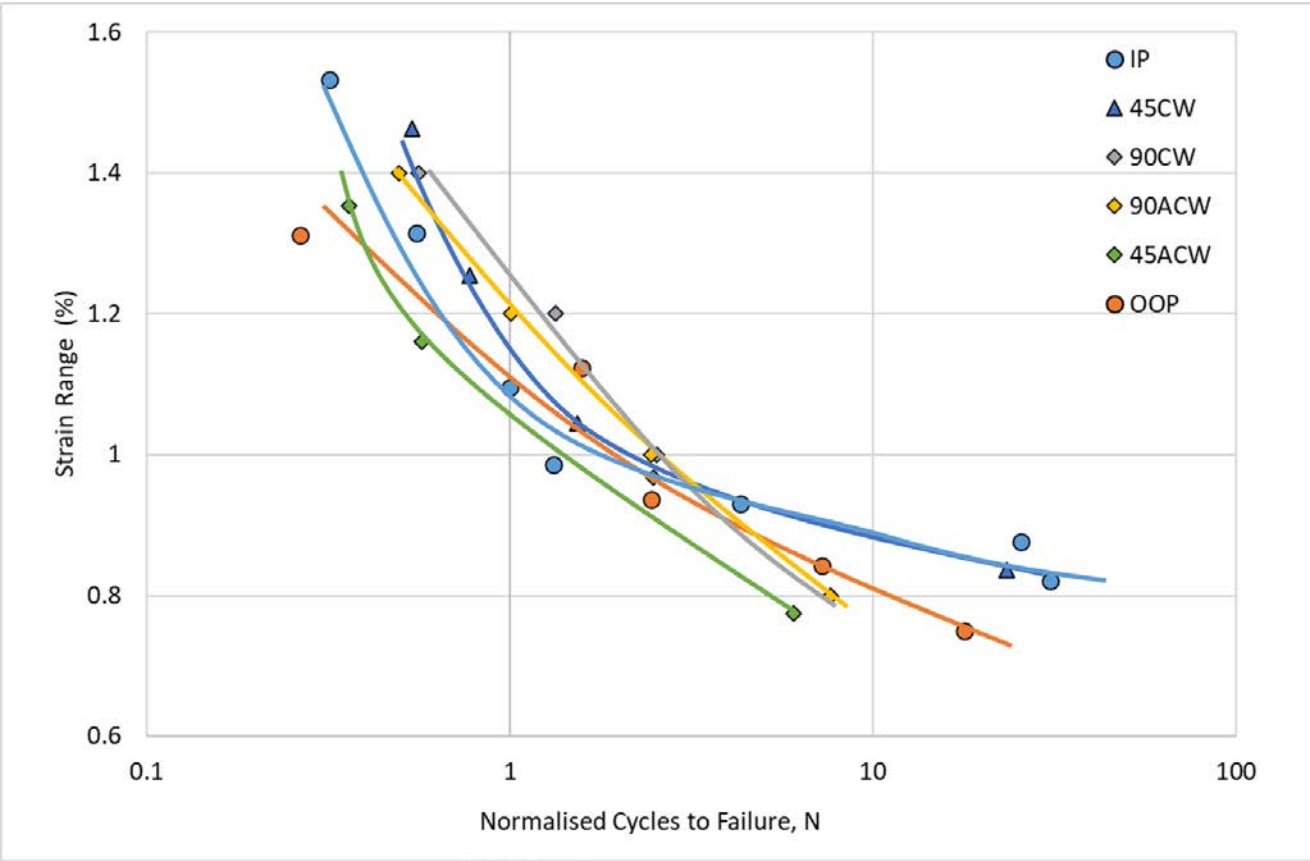

Figure 10: SC-TMF Phase Temperature Modified Strain vs. Life

The next step is to identify the threshold within the data that TMF phasing has the most significant impact on life. To analyse the modified strain TMF life, a Coffin-Manson style relationship was fitted to Figure 10:

$$\Delta\varepsilon(T_\varphi) = A(N_f)^b \tag{8}$$

This relationship provides a good fit for all phase angles, except the IP and 45CW. When these two specific phase angles are considered, their curve shape more closely reflects a Basquin and Coffin-Manson relationship. This arises from the small amount of plasticity seen at low strains coupled with these phase angles having T_{max} at σ_{max} i.e. maximum ductility at σ_{max}. Figure 11 uses the modified strain values and shows the Coffin-Manson fit for all phase angles and the Basquin-Coffin-Manson fit for the IP and 45CW angles.

a)

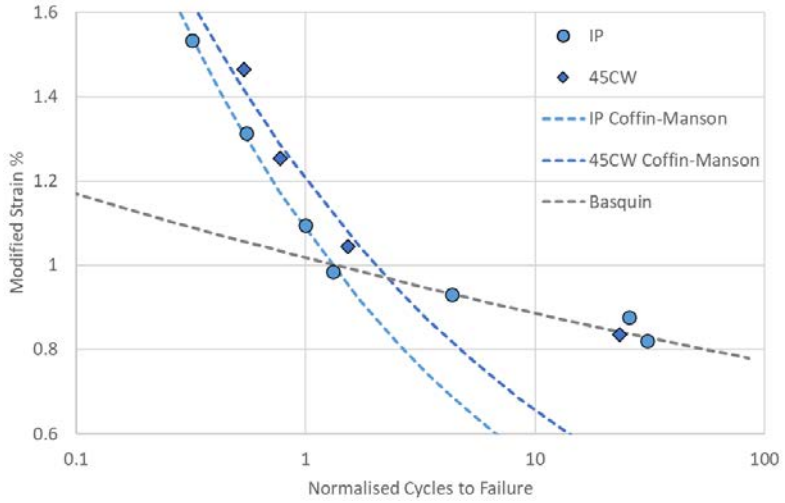
1.6
1.4
1.2
1
0.8
0.6
Modified Strain %
0.1
1
10
100
Normalised Cycles to Failure
IP
45CW
IP Coffin-Manson
45CW Coffin-Manson
Basquin

b)

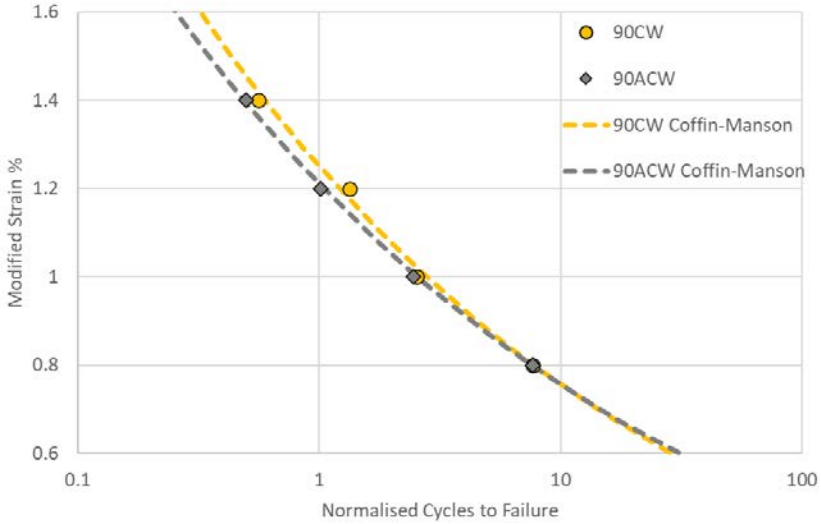
1.6
1.4
1.2
1
0.8
0.6
Modified Strain %
0.1
1
10
100
Normalised Cycles to Failure
90CW
90ACW
90CW Coffin-Manson
90ACW Coffin-Manson

c)

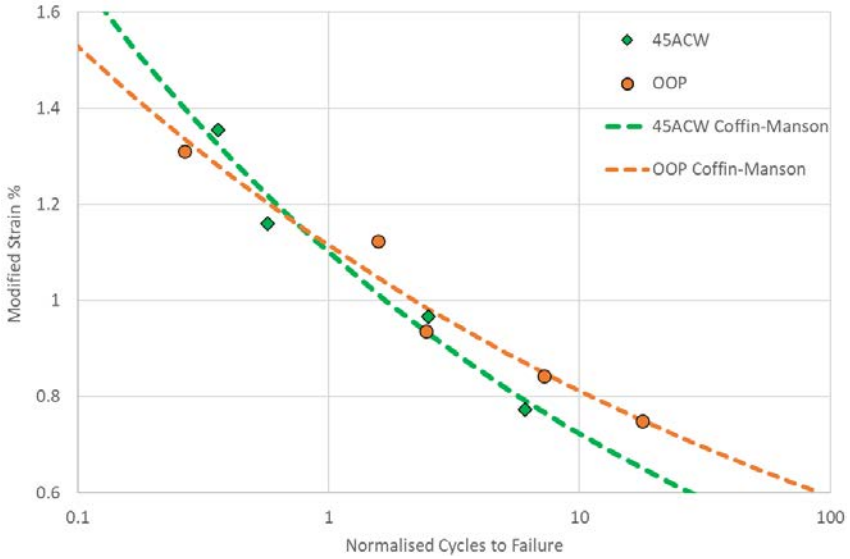
1.6
1.4
1.2
1
0.8
0.6
Modified Strain %
0.1
1
10
100
Normalised Cycles to Failure
45ACW
OOP
45ACW Coffin-Manson
OOP Coffin-Manson

Figure 11: Fitting of Coffin-Manson relationship to Modified Strain SC-TMF: a) IP and 45CW Basquin and Coffin-Manson b) 90CW and 90ACW, and c) 45ACW and OOP

Considering the fitted constants for only the fitted Coffin-Manson relationship using the modified strain term, a clear relationship becomes apparent between phase angle and life. In Figure 12 the fitted A and b coefficients are shown with regards to phase angle. Both coefficients create a linear relationship between IP and OOP phase angles.

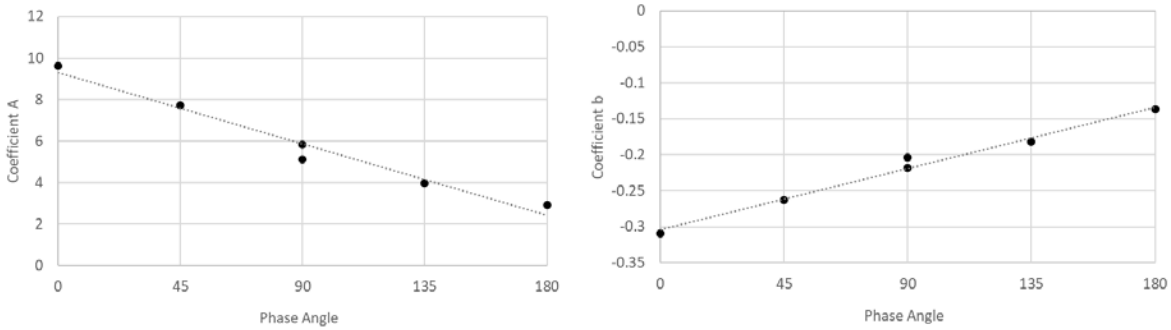

Figure 12: Relationship of Coffin-Manson Coefficients to Phase Angle: a) Coefficient A, and b) Coefficient b

5. Discussion

Taking a holistic approach to TMF by drawing together LC and SC-TMF results and microstructural observations, a more sophisticated understanding of TMF life and phase angle has been developed.

IP TMF sees ε_{max} occur at T_{max}. As the tensile stress opens the crack, the high temperature encourages oxygen diffusion that consequently forms preferentially on the grain boundaries. This results in the formation of an oxide wedge at the crack tip and oxide weakened grain boundaries, along which crack growth is therefore accelerated.

Considering the alternate case of OOP TMF, it behaves closer to observed isothermal fatigue undergoing crack propagation and transgranular failure. The reduced influence of oxidation can be attributed to its occurrence at the minimum stress (σ_{min}). For OOP TMF this means oxidation primarily occurs after the crack has closed, maintaining the sharpness of the crack tip and promoting propagation along the transgranular {111} plane. As the crack is under compression when this oxidation occurs the oxygen is unable to diffuse sufficiently far to impact the crack tip. This is supported by the Paris constants of OOP matching those of isothermal vacuum dwell tests [24], strongly indicating that T_{max} at σ_{min} reduces the impact oxidation has on total life.

The current analysis of both crack initiation and propagation under TMF loading is relatively unique since datasets of this type are currently very limited. The current work has allowed for not only consideration of a total life approach, but also the effect

of phase angle on TMF life. In particular it is important that a predictive methodology has been derived which allows for the consideration of intermediate phase angles using continuous functions. Traditionally IP and OOP datasets are generated with a lesser amount of information available on 90CW and 90ACW phase angles. However, any gas turbine components experience in servie environments which align more closely to 45ACW TMF cycles, and as such the methodology here allows for consideration of this behaviour. Furthermore, having developed a relationship to predict the TMF life of interim phase angles from IP and OOP tests, it is possible to apply it to existing datasets in the literature. Previously mentioned, work by Guth *et al.* [14] on Mar-M247 featured life data for $\Delta\varepsilon$=0.3-0.6% IP, 90CW, 90ACW and OOP with T=100-850°C. Using temperature dependant elastic modulus data from [25] and [26] the described procedure was conducted to predict the life of the 90CW/90ACW life as shown in Figure 13. The model more accurately predicts the 90CW/90ACW life to be greater than the IP and OOP over the same strain range. The model is most accurate over the data range also covered by IP and OOP data.

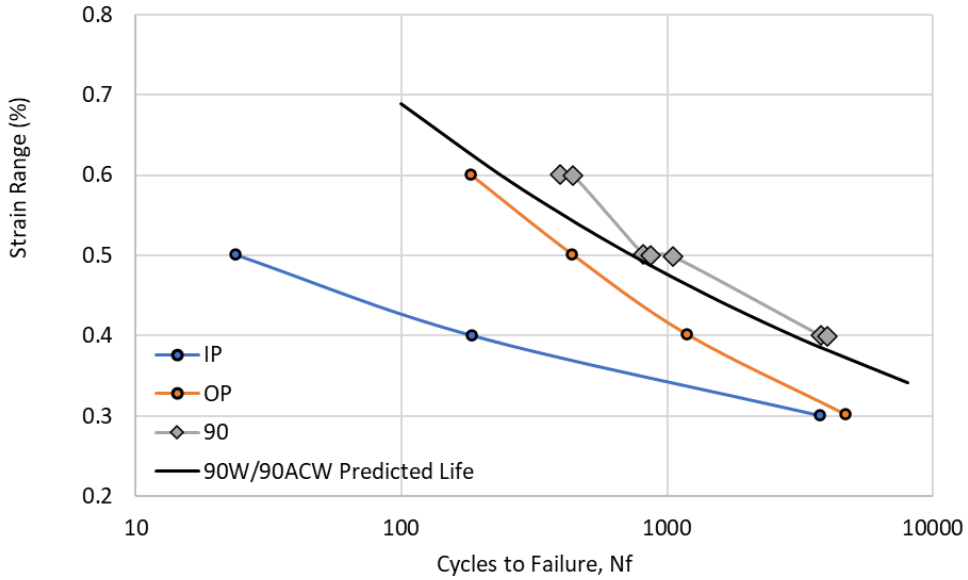

Figure 13: Predicting TMF life of 90CW and 90ACW for Mar-M247

For P92 steel, Pan *et al.* also conduct IP, OOP and 90CW TMF tests for $\Delta\varepsilon$=0.4-0.8% and T=550-650°C [27]. Temperature dependant elastic modulus data was taken from [28]. Figure 14 shows actual and predicted 90CW/90ACW life from IP and OOP using the described method. The model more predicts the 90CW/90ACW life to be less than the OOP and greater than the IP over the same strain range. Again, the model is most accurate over the data range also covered by IP and OOP data i.e. low strain range.

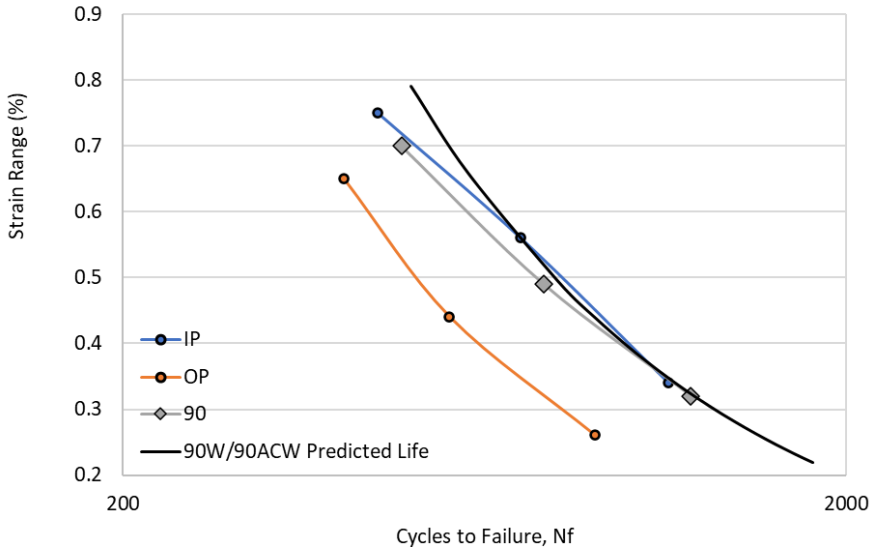

Figure 14: Predicting TMF life of 90CW for P92

Conclusions

TMF testing is complex, requiring advanced knowledge and sophisticated equipment. The current research landscape focuses on mainly IP and OOP TMF without much consideration for crucial intermediate phases such as 45ACW which best represents the conditions experienced by many gas turbine components. The work presented here takes a holistic approach building a more sophisticated understanding surrounding crack development and failure in a dynamic environment. By taking a holistic approach to TMF, this work collates the microstructural mechanisms and behaviour of RR1000 and develops a model to predict its behaviour under TMF conditions. This work has taken into account the impact of the thermal cycle i.e. phase angle by developing a modified strain to reflect the elastic modulus at maximum strain. A Coffin-Manson style relationship was then fitted with coefficients that are linear functions of phase angle. From the model presented, it is possible to accurately predict interim TMF phase angle life from IP and OOP data only. It also suggests that once A and b have been defined there is an ability to extrapolate this data to higher strains.

The role of IP TMF is critical in crack initiation and intergranular failure. For OOP, more typical isothermal style propagation and transgranular failure is seen. From this understanding a model has been proposed which has the capability to predict the impact of phase angle on TMF life. By using a modified strain term, this model can accurately predict all phase angles from IP and OOP results.

Acknowledgements

This work was funded under the EPSRC Rolls-Royce Strategic Partnership in Structural Metallic Systems for Gas Turbines (grants EP/H500383/1 and EP/H022309/1). The provision of materials and technical support from Rolls-Royce plc. is gratefully acknowledged.

References

[1] P Zhang, Q Zhu, G Chen, and C Wang, *Review on Thermo-Mechanical Fatigue Behaviour of Nickel-Base Superalloys*, Materials Transactions **56**(12), pp.1930-1939, 2015.

[2] DL McDowell, SD Antolovich, and RLT Oehmke, *Mechanistic consideration for TMF life prediction of nickel-base superalloys*, Nuclear Engineering and Design **133**, pp.383-399, 1992.

[3] M Marchionni, H Klingelhöffer, HJ Kühn, T Ranucci, and K Matzak, *ThermoMechanical Fatigue of the Nickel–Base Superalloy Nimonic 90,* Key Engineering Materials **345**, pp.347–350, 2007.

[4] S Pahlavanyali, G Drew, A Rayment, and C Rae, *Thermo-mechanical fatigue of a polycrystalline superalloy: The effect of phase angle on TMF life and failure*, International Journal of Fatigue **30**(2), pp.330–338, 2008.

[5] Z Huang, Z Wang, S Zhu, F Yuan, and F Wang, *Thermomechanical fatigue behavior and life prediction of a cast nickel-based superalloy*, Materials Science and Engineering A **432**(1), pp.308–316, 2006.

[6] CJ Hyde, W Sun, and TH Hyde, *An investigation of the failure mechanisms in high temperature materials subjected to isothermal and anisothermal fatigue and creep conditions*, Engineering **10**, pp.1157–1162, 2011.

[7] CJ Hyde, W Sun, TH Hyde, and AA Becker, *The Effect of a Starter Notch on the Isothermal and Thermomechanical Fatigue Life of a Nickel-Based Superalloy*, in ASME 2010 Pressure Vessels & Piping Division / K-PVP Conference, Washington USA, pp.1–10, 2010.

[8] R Lancaster, MT Whittaker and SJ Williams, *A review of thermo-mechanical fatigue behaviour in polycrystalline nickel superalloys for turbine disc applications*, Materials at High Temperatures **30**(1), pp.2-12, 2013.

[9] J Jones, MT Whittaker, R Lancaster, and S Williams, *Lifing the thermo-mechanical fatigue (TMF) behaviour of the polycrystalline nickel-based superalloy RR1000,* MATEC Web of Conferences, January 2014.

[10] MT Whittaker, R Lancaster, W Harrison, CJ Pretty and SJ Williams, *An Empirical Approach to Correlating Thermo-Mechanical Fatigue Behaviour of a Polycrystalline Ni-Base Superalloy*, Materials **6**(11), pp.5275-5290, 2013.

[11] CJ Pretty, MT Whittaker and SJ Williams, *Thermo-Mechanical Fatigue Crack Growth of RR1000*, Materials **10**(1), 2017

[12] J Palmer, J Jones, A Dyer, R Smith, R Lancaster and MT Whittaker, *Development of test facilities for thermo-mechanical fatigue testing*, International Journal of Fatigue **121**, pp.208-218, 2019.

[13] J Jones, MT Whittaker, R Lancaster, C Hyde, J Rouse, B Engel, S Pattison, S Stekovic, C Jackson and HY Li, *The effect of phase angle on crack growth mechanisms under thermo-mechanical fatigue loading*, International Journal of Fatigue **135**, 2020.

[14] S Pahlavanyali, G Drew, A Rayment, CMF Rae, "Thermo-mechanical fatigue of a polycrystalline superalloy: The effect of phase angle on TMF life and failure", International Journal of Fatigue, Volume 30, Issue 2, 2008,Pages 330-338.

[15] S Guth, S Doll, K-H Lang, "Influence of phase angle on lifetime, cyclic deformation and damage behavior of Mar-M247 LC under thermo-mechanical fatigue", Materials Science and Engineering: A, Volume 642, 2015, pp 42-48.

[16] S Guth, K-H Lang, "An approach to lifetime prediction for a wrought Ni-base alloy under thermo-mechanical fatigue with various phase angles between temperature and mechanical strain", International Journal of Fatigue, Volume 99, Part 2, 2017, pp 286-294.

[17] P Hahner, C Rinaldi, V Bicego, E Affeldt, T Brendel, H Andersson, et al."Research and development into a European code of practice for strain controlled thermo-mechanical fatigue testing" Int J Fatigue, 30 (2) (2008), pp. 372-381

[18] J Jones, MT Whittaker, R Lancaster and SJ Williams, *The influence of phase angle, strain range and peak cycle temperature on TMF crack initiation behaviour and damage mechanisms of nickel-based superalloy, RR1000*, International Journal of Fatigue **98**, pp.279-285, 2017.

[19] E Duffy, *The Constitutive Behaviour of a Nickel-based Superalloy*, PhD Thesis, Swansea University, 2017.

[20] J Zhang, XD He, Y Sha and SY Du, *The compressive stress effect on fatigue crack growth under tension-compression loading*, International Journal of Fatigue **33**(2), pp.361-367, 2010.

[21] MT Whittaker, RJ Lancaster, W Harrison, CJ Pretty, S Williams "An Empirical Approach to Correlating Thermo-Mechanical Fatigue Behaviour of a Polycrystalline Ni-Base Superalloy" Materials. 2013; 6(11):5275-5290.

[22] A Karabela, L Zhao, J Tong, N Simms, J Nicholls and M Hardy, *Effects of cyclic stress and temperature on oxidation damage of a nickel-based superalloy*, Materials Science and Engineering A **528**(19), pp.6194-6202, 2011.

[23] Z Mróz, "An attempt to Describe the Behaviour of Metals under Cyclic Loads Using a More General Workhardening Model", Acta Mechanica **7**, pp.199-212, 1969.

[24] JH O'Hanlon, M Hardy, DJ Child, B Foss, PJ Withers and M Bache, *The effect of minimum dwell cycles on the environmental and fatigue response of RR1000*, MATEC Web of Conferences, January 2014.

[25] S Chen, S Su and W Jehng "Characterization of shear stresses in nickel-based superalloy Mar-M247 when orthogonal machining with coated carbide tools" Journal of Central South University, 2014, Vol. 21, pp 862-869

[26] K.A. Brindley "Thermomechanical fatigue of Mar-M247: Extension of a constitutive and life model to higher temperatures" PhD thesis, Georgia Institute of Technology, May 2014.

[27] X Pan, X Li, L Chang, G Zhang, F Xue, Y Zhao, C Zhou, "Thermal-mechanical fatigue behavior and lifetime prediction of P92 steel with different phase angles", International Journal of Fatigue, Vol 109, 2018, pp 126-136

[28] Sehitoglu, H. and Boismier, D. A., "Thermo-mechanical fatigue of MarM247: Part 2—life prediction," Journal of Engineering Materials and Technology, vol. 112, pp. 80–89, January 1990.